Acoustic Scattering Mediated Single Detector Optoacoustic Tomography

X. Luís Deán-Ben,[1,2,3,*] Ali Özbek,[1,2,3] Hernán López-Schier,[4] and Daniel Razansky[1,2,3,5]
[1]Faculty of Medicine and Institute of Pharmacology and Toxicology, University of Zürich, CH-8057 Zürich, Switzerland
[2]Institute for Biomedical Engineering and Department of Information Technology and Electrical Engineering, ETH Zurich, CH-8093 Zürich, Switzerland
[3]Institute for Biological and Medical Imaging, Helmholtz Zentrum München, D-85764 Neuherberg, Germany
[4]Research Unit Sensory Biology and Organogenesis, Helmholtz Zentrum München, D-85764 Neuherberg, Germany
[5]School of Medicine, Technische Universität München (TUM), D-81675 Munich, Germany

(Received 31 March 2019; published 25 October 2019)

Optoacoustic image formation is conventionally based upon ultrasound time-of-flight readings from multiple detection positions. Herein, we exploit acoustic scattering to physically encode the position of optical absorbers in the acquired signals, thus reducing the amount of data required to reconstruct an image from a single waveform. This concept is experimentally tested by including a random distribution of scatterers between the sample and an ultrasound detector array. Ultrasound transmission through a randomized scattering medium was calibrated by raster scanning a light-absorbing microparticle across a Cartesian grid. Image reconstruction from a single time-resolved signal was then enabled with a regularized model-based iterative algorithm relying on the calibration signals. The signal compression efficiency is facilitated by the relatively short acquisition time window needed to capture the entire scattered wave field. The demonstrated feasibility to form an image using a single recorded optoacoustic waveform paves a way to the development of faster and affordable optoacoustic imaging systems.

DOI: 10.1103/PhysRevLett.123.174301

Optoacoustic (OA) (photoacoustic) imaging has enabled breaking through the light diffusion barrier to map optical contrast (absorption) with high resolution deep into living organisms [1–3]. This is achieved by capitalizing on the low scattering of ultrasound, as compared to that of light, in soft biological tissues. A myriad of OA systems based on single detector scanning as well as simultaneous acquisition of tomographic information using array detectors have been suggested [4]. In all cases, image formation is based on the assumption that ultrasound waves undergo no distortion and propagate with constant velocity across the sample and coupling medium (typically water). Internal reflections and acoustic scattering may severely deteriorate the quality of the rendered images and, thus, generally have to be avoided [5,6].

A consequence of acoustic reflections and scattering is the appearance of late responses in the collected time-resolved signals, leading to arc-type artifacts and overall distortion in OA images [7]. Such late responses may nevertheless contain useful information. For example, acoustic reflectors have been included in OA tomographic imaging systems to maximize the effective angular coverage and avoid so-called limited-view effects [8,9]. The late parts of OA signals corresponding to reflected waves can in fact be considered as additional signals collected from mirrored locations, thus effectively doubling the amount of information contained in each signal acquisition. In this way, additional information associated to acoustic reflections can effectively be used to reduce the number of signals required for image formation. Ideally, a single recorded waveform would encode the location of multiple absorbers, provided that a sufficient number of reflected waves is acquired. Physical compression of the location of sources in a single waveform is facilitated by the fact that the propagation of waves in a linear medium is deterministic and not random, regardless of the complexity of the medium. This enables physically or numerically time reversing the wave field to refocus the wave at the location of the sources [10]. This principle has been previously exploited in several fields such as radio frequency communication [11], ultrasound imaging and focusing [12–14], light wave front shaping [15,16], or numerical reconstruction of optoacoustic images [17].

In this work, we suggest an approach to encode the location of light-absorbing structures in OA signals based on multiple scattering of ultrasound waves. For this, randomly distributed acoustic scatterers in front of a transducer array result in a unique complex propagation path for the ultrasound waves generated at each source location within the effective field of view. As a result, distinct optoacoustic waveforms are generated by absorbers located at different positions. The number of signals required for reconstructing an OA image can then be significantly reduced without considerably extending the acquisition time window.

A layout of the experimental system used to test the suggested concept is depicted in Fig. 1(a). A full-ring (360°) array of cylindrically focused transducers was

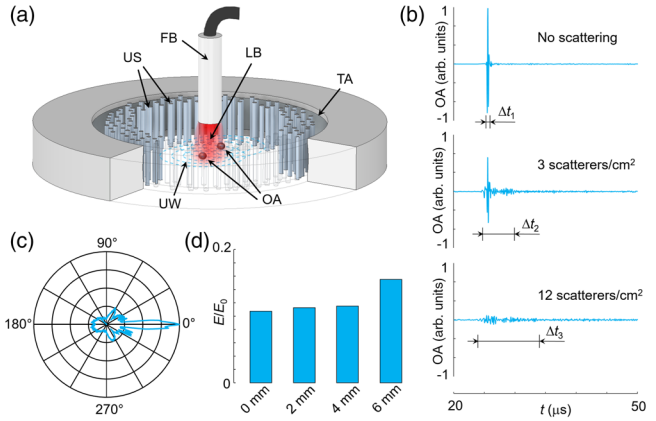

FIG. 1. Acoustic scattering of optoacoustic waves. (a) Layout of the experimental system. TA, transducer array; US, ultrasound scatterers; FB, fiber bundle; LB, laser beam; OA, optical absorbers; UW, ultrasound waves. (b) Collected optoacoustic signals with no scatterers in the propagating path, relatively low and high density of scatterers. (c) Scattered wave directivity for an individual scatterer located at a distance of 16.25 mm from a point absorber. (d) Ratio of the total detected OA signal energy with and without scatterers in the propagating path versus distance of the absorbing microsphere from the center of the transducer array. The signal energy is integrated over all transducer elements and time instants.

employed. The OA signals were generated by directly illuminating the region of interest (ROI) with a nanosecond pulsed laser at 720 nm wavelength. The OA signals detected by the array elements were digitized at 40 megasamples per second for a time window of 494 samples delayed by 20 μs with respect to the laser pulse. The OA acquisition window was adapted to cover the entire time-resolved signals considering that the first (unscattered) waves arrive $\sim$26 μs after emission of the laser pulse and that no significant acoustic reflections from the ring array were observed. The collected signals were bandpass filtered between 0.5–8 MHz to remove low-frequency offsets and high-frequency noise. A cluster of acoustic scatterers were randomly distributed along a circular ring coaxially aligned with the array. Specifically, $\sim$300 borosilicate capillary glass tubings with inside and outside diameters of 0.86 and 1.50 mm, respectively (Warner Instruments LLC, Hamden, USA) were distributed along an annulus with 16 mm radius and 20 mm thickness. The custom-made array (Imasonics SaS, Voray, France) has a radius of 40 mm and consists of 512 elements with 5 MHz central frequency and >80% detection bandwidth. The dimensions of the elements are 0.37×15 mm^2.

The effects of acoustic scattering in the collected OA signals are illustrated in Fig. 1(b). For a single 100-μm-diameter microsphere absorber (Cospheric LLC, Santa Barbara, CA), the signal detected by one of the array elements with no scatterers in the propagating path is plotted at the top. As expected, the generated signal is confined in time to a short interval corresponding to $\Delta t_1 \sim 1/\mathrm{BW}$ centered at $t = d/c$, where BW is the detection bandwidth, d is the distance between the sphere and the sensor, and c is the speed of sound. The other two plots show the detected signal when acoustic scatterers are present [Fig. 1(a)]. For the relatively low scattering density of 3 scatterers/cm^2, the signal extends in time over $\Delta t_2 \sim 5$ μs, yet the part corresponding to direct propagation remains dominant and contains most of the useable information for image reconstruction. Note also some early arriving responses ascribed to a direct acoustic propagation through glass having speed of sound significantly higher than water. The signal detected in the presence of densely distributed 12 scatterers/cm^2 exhibits a complex pattern spanning $\Delta t_1 \sim 10$ μs and has no dominant peaks. In this case, the location of the point absorber is encoded along the entire recorded interval; thus any given distribution of optical absorbers can potentially be compressed into a single waveform.

We next measured the directivity pattern for an individual scatterer by placing an absorbing microsphere at the center of the transducer array and a glass tubing at a distance of 16.25 mm from it. The relative amplitude of the scattered wave for different angles was estimated by measuring the difference between the OA signals collected by all the array elements with and without the tubing in the propagating path. Note that the scattering directivity pattern is generally defined as the scattered wave field from an incident plane wave. For the measurement performed, the distance between the absorbing microsphere is much larger than the diameter of the glass tubing and, hence, the incident wave front can be approximated as plane. It is shown that the scattered waves have a dominant forward propagation component. This is expected considering that the effective dimension of each scatterer corresponds to $\sim 5\lambda_a$ (λ_a being the acoustic wavelength at the central frequency of the detection array), which falls into the Mie scattering regime. Forward propagation is essential to minimize the loss of energy due to transmission through the scattering medium. Collecting signals with high energy is essential for both encoding sufficient information as well as for achieving a good signal-to-noise ratio (SNR) in the reconstructed images. Figure 1(d) shows the ratio of the total detected OA signal energy for all array elements with (E) and without (E_0) scatterers present in the propagating path. For our detection configuration approximately 10% of the OA signal energy is preserved after adding scattering. This value is increased for OA sources located away from the array's center, suggesting that cylindrical focusing of the detection elements contributes to the energy collection efficiency.

Image reconstruction in the presence of acoustic scattering implies establishing a model linking the initial OA pressure (proportional to the optical absorption) to the collected pressure waveforms. Similarly to the time-domain

model-based OA reconstruction approaches [18,19], one may assume that the absorbed energy is confined within the region of interest and that the acquired OA signals $p(r,t)$ correspond to a linear superposition of the signals $p_i(r,t)$ for each pixel belonging to the image grid covering such ROI, i.e.,

$$p(r,t) = \sum_i h_i p_i(r,t), \tag{1}$$

where h_i is the absorbed optical energy for the ith pixel. For ultrasound waves propagating through a uniform non-scattering medium, $p_i(r,t)$ can be estimated from the OA forward model, e.g., by interpolating light absorption values between the pixel positions [19]. When acoustic scattering takes place, physical modeling of $p_i(r,t)$ implies accurate knowledge of the position, shape, and acoustic properties of the scatterers, which may become too complicated. Instead, $p_i(r,t)$ can be experimentally measured by moving an OA source across a grid of points and collecting the corresponding responses. For this purpose, a 100 μm polyethylene microsphere was scanned with 75 μm steps in the horizontal and vertical directions over a ROI of 4.5×4.5 mm^2. For the experimentally measured signals, Eq. (1) represents a linear model that can be expressed in a matrix form via

$$\mathbf{p} = \mathbf{M}\mathbf{h}, \tag{2}$$

where $\mathbf{p}$ is a column vector containing the signal(s) for a set of positions and instants and $\mathbf{h}$ is a vector containing the absorbed energy in each pixel of the scanning grid. The columns of matrix $\mathbf{M}$ represent the time-resolved signal(s) for each position of the scanned particle. The signal(s) being considered may as well be obtained by adding up individual signals from multiple elements, in which case the model in Eq. (2) is equally valid. The performance of the model in Eq. (2) for image reconstruction from a reduced number of signals was first tested by considering a sparse distribution of absorbers. For this, the microsphere was scanned at random grid points within the ROI not included in the calibration grid. The OA signals from all transducer elements were added up to form a unique time-resolved signal expressed in a vector form as $\mathbf{p}_m$. Image reconstruction was based on numerical inversion of Eq. (2), i.e.,

$$\mathbf{h}_{\text{sol}} = \text{argmin}_{\mathbf{h}}\{\|\mathbf{p}_m - \mathbf{M}\mathbf{h}\|_2^2 + \lambda R(\mathbf{h})\}, \tag{3}$$

where the parameter λ allows weighting the regularization term $R(\mathbf{h})$. The fast iterative shrinkage thresholding algorithm (FISTA) [20] was used to split the inversion problem in Eq. (3) into two problems, namely a model inversion and a denoising problem. The denoising problem was solved using the primal-dual hybrid gradient method.

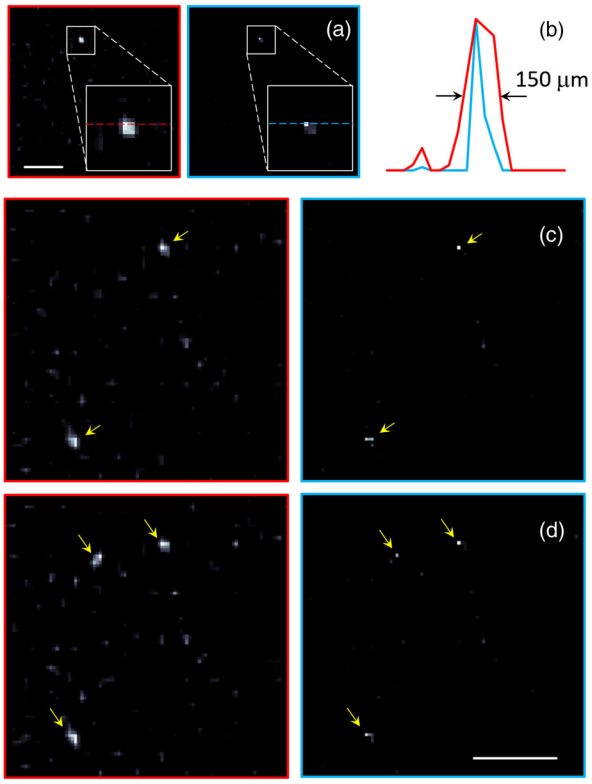

FIG. 2. Experimental validation of the scattering mediated single detector optoacoustic tomography. (a) Optoacoustic images of a microsphere reconstructed with a single detected waveform. (b) One-dimensional profiles along the reconstructed images shown in (a). Images reconstructed for 2 and 3 microspheres are shown in (c) and (d), respectively. The yellow arrows indicate the position of the spheres. Red and blue squares correspond to inversions done with either $L2$ or $L1$ norm [$l = 2$ or $l = 1$ in Eq. (3)]. Scale bars are 1 mm.

This approach enables reducing the number of model matrix multiplication operations, which represent the dominant computational load. The stopping criterion was based on the duality gap value. This, along with the regularization term, was heuristically selected based on image quality inspection. Approximately 5 iterations of FISTA and 128 iterations of primal or dual were required. The computations were implemented on an OpenCL framework and executed in a NVIDIA GeForce GTX TITAN X graphics processing unit (GPU). The reconstruction results for an individual microsphere obtained by taking standard Tikhonov regularization based on the $L2$ norm, i.e., $R(\mathbf{h}) = \|\mathbf{h}\|_2^2$ in Eq. (3), indicate that it was possible to accurately reconstruct an image of a point absorber with a single OA waveform [Fig. 2(a)]. The FWHM of the reconstructed sphere is ~150 μm, as indicated in the profile in Fig. 2(b), which matches the expected in-plane spatial resolution of the array for the scattering-free case. Images of microspheres obtained without the cluster of acoustic scatterers in the propagating path can be found in Ref. [21]. The profile in Fig. 2(b) corresponding to the image

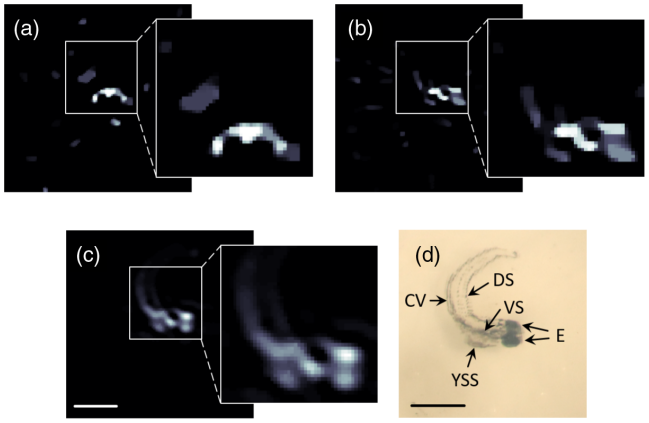

FIG. 3. Imaging of 5 days-post-fertilization zebrafish larva post mortem. (a) Optoacoustic image of the larva obtained with a single integrated waveform. (b) Optoacoustic image of the larva obtained from 16 individual signals. (c) Optoacoustic image of the larva obtained with all 512 signals from the transducer array with no acoustic scattering in the ultrasound propagating path. (d) Bright field microscopy image of the larva. E, eyes; YSS, yolk sac stripe; VS, ventral strip; DS, dorsal stripe; CV, caudal vein. Scale bars are 1 mm.

reconstructed considering the $L1$ norm, i.e., $R(\mathbf{h}) = \|\mathbf{h}\|_1$ in Eq. (3), has a significantly lower FWHM. This is attributed to the sparsity condition and must not necessarily be ascribed to the achievable resolution, although $L1$-based regularization has been shown to enhance the spatial resolution beyond the acoustic diffraction barrier [22]. Accurate reconstructions are similarly rendered when multiple microspheres are present in the ROI [Figs. 2(c) and 2(d)]. Higher noise levels are however produced due to the reduced sparsity of the images, which hampers image reconstruction from a single waveform.

The imaging performance of the suggested approach was further tested by imaging a wild-type zebrafish larva 5 days-post-fertilization post mortem. Image reconstruction was performed considering a total variation regularization term, i.e., $R(\mathbf{h}) = \|\nabla\mathbf{h}\|_1$ in Eq. (3). Reconstruction was performed by adding up signals from multiple elements of the array, which was shown to perform better than when considering individual signals. The image reconstructed from a signal corresponding to the sum of all 512 signals of the array renders the fish in the correct position, although its shape is distorted [Fig. 3(a)]. Clearly, the image quality improves when reconstructing with 16 signals corresponding to the sum of alternating channels of the array [Fig. 3(b)]. The condition numbers of the matrices used to reconstruct the images in Figs. 3(a) and 3(b) are 4.4×10^{15} and 257. These numbers give an estimate on how much the relative noise in the signals is amplified in the inversion problem. Considering a typical SNR of 32 dB (2.5% relative error due to noise) of the collected signals, it appears that the inversion problem is generally ill-conditioned and needs to be regularized. Equivalent condition numbers for the matrices built from 1 and 16 signals of individual elements of the array are 5.0×10^{15} and 307, respectively. As a reference, Fig. 3(c) shows the image reconstructed with all the 512 array elements with no scatterers in the ultrasound propagating path and Fig. 3(a) shows a bright field microscopic image of the larva, where relatively large light absorbing structures are labeled. For the reconstruction of the image in Fig. 3(c), a conventional model matrix $\mathbf{M}$ was built as described elsewhere [23]. Even though the reference image exhibits the best reconstruction quality, most structures can be clearly identified in images reconstructed with a significantly lower number of signals.

Minimization of the amount of data required for OA image formation may contribute to reducing costs or, alternatively, speeding up acquisitions. Herein, we have demonstrated the basic feasibility to "physically" encode the optical absorption distribution in a defined ROI by capitalizing on the complex propagation of ultrasound waves in a scattering medium. While several time-of-flight readings are normally required to trilaterate the position of a given OA source, this information can alternatively be carried via multiple acoustic scattering events. Thus, the suggested approach represents a sort of compressed data acquisition methodology. Note that OA modeling is facilitated by the fact that individual sources generate known bipolar signals with a defined shape, in a way that the collected signals are not affected by random speckle noise [24]. Accurate OA images have been achieved with model-based inversion methods with no regularization or by incorporating standard linear regularization terms [25]. Herein, we have shown that imposing a sparsity condition with a $L1$-based regularization term, as generally done in compressed-sensing-based reconstruction, greatly facilitates image reconstruction. Optimal regularization depends on the specific imaging scenario [26]. In the suggested approach, the regularization term must be established as a function of the OA acquisition geometry, the distribution of acoustic scatterers, as well as the specific features of the sample, which determine the condition of the model matrix. In a conventional OA imaging scenario, temporal resolution is ultimately limited by the time it takes for all the generated signals to leave the ROI. While this ultimate limit is unattainable with the suggested approach due to the extended acquisition window caused by multiple scattering events, such a window is much shorter than that required for alternative approaches using acoustic reflectors [8].

An important aspect to consider is the required duration of the scattered wave field in the acquired time-resolved signal(s) so that sufficient information is encoded to reconstruct an arbitrary image. It has been established that all eigenmodes in a ergodic cavity can be built by interference of the multireflected waves induced by the time-reversed signal at a single point with a duration larger than the Heisenberg time [27]. Similarly, the number of

uncorrelated speckle fields in the reconstruction region of interest that are transmitted within the signal bandwidth can be considered for wave propagation through a scattering medium [27]. For a single signal, this is equivalent to the number $N \sim \Delta T \Delta f$ of uncorrelated frequencies, where ΔT is the time duration of such a signal and Δf its bandwidth. Taking $\Delta T \sim 10$ μs and $\Delta f \sim 5$ MHz, $N \sim 50$ uncorrelated pixels can be recovered. Considering an expected resolution of 150 μm, an arbitrary image can then potentially be reconstructed for a field of view of 1.05×1.05 mm^2. For larger fields of view, the reconstruction falls into the compressed sensing class of problems, unless a longer time duration or several signals are considered. The diffuse approximation can be used to approximate the time duration of the scattered wave field in the multiscattering regime as the Thouless time L^2/D, where L is the thickness of the medium and D the diffusion coefficient [15].

A potential drawback of the suggested methodology is the limited data sparsity, which is essential for high-quality OA image reconstruction. We have shown that a single absorber can be very accurately reconstructed with a single waveform, which is more challenging for multiple sources. Yet, individual flowing absorbers have been previously used in localization OA tomography to break through the acoustic diffraction barrier [28,29]. Therefore, compressed acquisition of signals may find applicability for super-resolution imaging of vascular structures. Similar methods have also been suggested for compressed acquisition of signals and reconstruction of sparse images in pulse-echo ultrasound [12,30]. A distribution of acoustic scatterers similar to the one employed here can thus serve the same purpose while also facilitating hybridization of ultrasonography with OA imaging. Overall, the demonstrated feasibility to form an image with a single OA waveform paves a way to the development of faster and affordable OA imaging systems.

This study was partially supported by the European Research Council Consolidator Grant No. ERC-2015-CoG-682379.

*Corresponding author.
xl.deanben@pharma.uzh.ch

[1] P. Beard, Biomedical photoacoustic imaging, Interface Focus **1**, 602 (2011).
[2] A. Taruttis and V. Ntziachristos, Advances in real-time multispectral optoacoustic imaging and its applications, Nat. Photonics **9**, 219 (2015).
[3] X. L. Deán-Ben, S. Gottschalk, B. Mc Larney, S. Shoham, and D. Razansky, Advanced optoacoustic methods for multiscale imaging of *in vivo* dynamics, Chem. Soc. Rev. **46**, 2158 (2017).
[4] L. V. Wang and J. Yao, A practical guide to photoacoustic tomography in the life sciences, Nat. Methods **13**, 627 (2016).
[5] X. L. Dean-Ben, R. Ma, D. Razansky, and V. Ntziachristos, Statistical approach for optoacoustic image reconstruction in the presence of strong acoustic heterogeneities, IEEE Trans. Med. Imaging **30**, 401 (2011).
[6] J. Poudel, T. P. Matthews, L. Li, M. A. Anastasio, and L. V. Wang, Mitigation of artifacts due to isolated acoustic heterogeneities in photoacoustic computed tomography using a variable data truncation-based reconstruction method, J. Biomed. Opt. **22**, 041018 (2017).
[7] X. L. Deán-Ben, V. Ntziachristos, and D. Razansky, Artefact reduction in optoacoustic tomographic imaging by estimating the distribution of acoustic scatterers, J. Biomed. Opt. **17**, 110504 (2012).
[8] B. T. Cox, S. R. Arridge, and P. C. Beard, Photoacoustic tomography with a limited-aperture planar sensor and a reverberant cavity, Inverse Probl. **23**, S95 (2007).
[9] B. Huang, J. Xia, K. I. Maslov, and L. V. Wang, Improving limited-view photoacoustic tomography with an acoustic reflector, J. Biomed. Opt. **18**, 110505 (2013).
[10] M. Fink, D. Cassereau, A. Derode, C. Prada, P. Roux, M. Tanter, J.-L. Thomas, and F. Wu, Time-reversed acoustics, Rep. Prog. Phys. **63**, 1933 (2000).
[11] A. Derode, A. Tourin, J. de Rosny, M. Tanter, S. Yon, and M. Fink, Taking Advantage of Multiple Scattering to Communicate with Time-Reversal Antennas, Phys. Rev. Lett. **90**, 014301 (2003).
[12] G. Montaldo, D. Palacio, M. Tanter, and M. Fink, Time reversal kaleidoscope: A smart transducer for three-dimensional ultrasonic imaging, Appl. Phys. Lett. **84**, 3879 (2004).
[13] T.-D. Luong, T. Hies, and C.-D. Ohl, A compact time reversal emitter-receiver based on a leaky random cavity, Sci. Rep. **6**, 36096 (2016).
[14] J. Robin, A. Simon, B. Arnal, M. Tanter, and M. Pernot, Self-adaptive ultrasonic beam amplifiers: Application to transcostal shock wave therapy, Phys. Med. Biol. **63**, 175014 (2018).
[15] A. P. Mosk, A. Lagendijk, G. Lerosey, and M. Fink, Controlling waves in space and time for imaging and focusing in complex media, Nat. Photonics **6**, 283 (2012).
[16] R. Horstmeyer, H. Ruan, and C. Yang, Guidestar-assisted wavefront-shaping methods for focusing light into biological tissue, Nat. Photonics **9**, 563 (2015).
[17] B. E. Treeby and B. T. Cox, k-wave: Matlab toolbox for the simulation and reconstruction of photoacoustic wave fields, J. Biomed. Opt. **15**, 021314 (2010).
[18] G. Paltauf, J. A. Viator, S. A. Prahl, and S. L. Jacques, Iterative reconstruction algorithm for optoacoustic imaging, J. Acoust. Soc. Am. **112**, 1536 (2002).
[19] A. Rosenthal, D. Razansky, and V. Ntziachristos, Fast semi-analytical model-based acoustic inversion for quantitative optoacoustic tomography, IEEE Trans. Med. Imaging **29**, 1275 (2010).
[20] A. Beck and M. Teboulle, A fast iterative shrinkage-thresholding algorithm for linear inverse problems, SIAM J. Imaging Sci. **2**, 183 (2009).
[21] E. Merčep, J. L. Herraiz, X. L. Deán-Ben, and D. Razansky, Transmission–reflection optoacoustic ultrasound (tropus) computed tomography of small animals, Light Sci. Appl. **8**, 18 (2019).

[22] D. M. Egolf, R. K. W. Chee, and R. J. Zemp, Sparsity-based reconstruction for super-resolved limited-view photoacoustic computed tomography deep in a scattering medium, Opt. Lett. **43**, 2221 (2018).
[23] X. L. Dean-Ben, V. Ntziachristos, and D. Razansky, Acceleration of optoacoustic model-based reconstruction using angular image discretization, IEEE Trans. Med. Imaging **31**, 1154 (2012).
[24] X. L. Deán-Ben and D. Razansky, On the link between the speckle free nature of optoacoustics and visibility of structures in limited-view tomography, Photoacoustics **4**, 133 (2016).
[25] A. Rosenthal, V. Ntziachristos, and D. Razansky, Acoustic inversion in optoacoustic tomography: A review, Curr. Med. Imaging Rev. **9**, 318 (2013).
[26] A. Chambolle and T. Pock, An introduction to continuous optimization for imaging, Acta Numer. **25**, 161 (2016).
[27] M. Fink, Time-reversal acoustics in complex environments, Geophysics **71**, SI151 (2006).
[28] S. Vilov, B. Arnal, and E. Bossy, Overcoming the acoustic diffraction limit in photoacoustic imaging by the localization of flowing absorbers, Opt. Lett. **42**, 4379 (2017).
[29] X. L. Dean-Ben and D. Razansky, Localization optoacoustic tomography, Light Sci. Appl. **7**, 18004 (2018).
[30] P. Kruizinga, P. van der Meulen, A. Fedjajevs, F. Mastik, G. Springeling, N. de Jong, J. G. Bosch, and G. Leus, Compressive 3D ultrasound imaging using a single sensor, Sci. Adv. **3**, e1701423 (2017).